*A. Fonner, S. C. Jana**

School of Polymer Science and Polymer Engineering, University of Akron, Akron, OH, USA

Investigation of Microstructures and Air Permeability of Aerogel-Coated Textile Fabric Materials

This study focuses on fabrication of aerogel-coated macroporous polyester fabrics for the purposes of filtration of nanometric airborne particles and potential application in facemasks. Syndiotactic polystyrene (sPS) and polyimide (PI) gels that provide respectively majority macropores (diameter > 50 nm) and mesopores (diameter 2 to 50 nm) are coated onto woven polyester fabrics via a dip coating process. The resultant materials are supercritically dried to obtain aerogel-coated fabrics. The results show that sPS is more suitable for the dip coating process. However, evaporation of the solvent during handling of gel-coated fabrics leads to closure of the surface pores that are later recovered via solvent annealing. The resultant aerogel-coated fabrics offer high air permeability ($\sim 10^{-10}$ m^2) and high filtration efficiency (> 99.95 %) of airborne sodium chloride test particles of size 25 to 150 nm.

1 Introduction

The ingress of airborne suspended particles into human body during inhalation process presents obvious health risks. This is especially true in the context of airborne nanometer size Covid-19 respiratory viruses spreading and causing the current pandemic. In view of this, the design of personal protective equipment for fight against airborne viruses must consider the specific size of the viruses for possible size-exclusion through porous media with close to 100 % retention capability while maintaining enough air permeability for breathing purposes. However, the pore size and air permeability cannot be independently tuned in spun fiber-based filter media, e. g., large pores and high porosity are needed for high air permeability while high removal efficiency is strictly dependent on the small size of pores that cannot be achieved simultaneously with a high level of porosity.

Prior work by Jana and coworkers (Kim et al., 2015; 2016; Kim and Jana, 2017; Kim et al., 2017; Zhai and Jana, 2017) built on limited knowledge available from existing patents and peer-reviewed publications on the topic (Robert and Jose, 2008; Alexander, 1992; Guise et al., 2001; Quevedo et al., 2008; Zebida, 2011) and showed that polymeric aerogel materials are able to decouple the inverse relationship of air permeability and particle removal efficiency. These authors evaluated the role of appropriate combinations of interconnected mesopores (diameter 2 to 50 nm) and macropores (diameter > 50 nm) to achieve high filtration efficiency, close to 99.995 % and air permeability of the order of 10^{-10} m^2. Zebida (2011) impregnated glass fiber mats with silica aerogel to improve filtration of airborne particles as small as 200 nm in diameter. Kim et al. (2015) reported that syndiotactic polystyrene (sPS) aerogel monoliths can be successfully used in removing airborne sodium chloride nanoparticles of diameter 25 to 50 nm with 99.95 % efficiency while maintaining air permeability at 10^{-10} m^2. Kim et al. (2016) analyzed the contributions of mesopores and macropores on filtration performance and established that mesopores are primarily responsible for airborne nanoparticle removal efficiency, while air permeability is reliant of the fraction of macropores, typically 200 nm or larger in diameter. These authors grew mesoporous silica gels in the macropores of sPS gels to vary independently the volume fractions of meso- and macropores. Kim and Jana (2017) observed significant dense skin layer formation in sPS aerogels during fabrication of filter media and reported that such skin layers serve as impediment to air permeability. The presence of α- and γ-form crystalline polyvinylidene fluoride (PVDF) fibrils in sPS aerogels with PVDF to sPS mass ratio of 0.06 to 1.7 helped increase the filtration efficiency to ≥ 99.999 % without affecting air permeability. Such an increase of filtration efficiency was attributed to electrostatic charge development in the aerogel filter media by PVDF. These concepts were later extended to polyimide aerogels by Zhai and Jana (2017) to show a direct relationship of macropore content and air permeability and mesopore content and filtration efficiency. In all cases, the filtration efficiency of airborne nanoparticles of diameter 25 to 150 nm (mean size 75 nm) was more than 99.995 % with air permeability of the order of 10^{-10} m^2.

Several independent studies on the use of aerogel materials for air filtration were reported by other research groups. Mosanenzadeh et al. (2020) studied the influence of an acylchloride crosslinker on development of mesoporous networks in polyimide aerogels and achieved air permeability of $\sim 10^{-10}$ m^2. These authors did not report filtration efficiency. Zhang et al. (2018) considered hydroxyapatite nanowire-based aerogels for air filtration of particles 2.5 mm or smaller. Zeng et al. (2019) prepared lignin-based aerogel materials by freeze drying and evaluated their potential as filter media for removal of ultrafine particles of diameter smaller than 100 nm.

* Mail address: Sadhan C. Jana, School of Polymer Science and Polymer EngineeringUniversity of Akron, 250 South Forge Street, Akron, OH 44325-0301, USA
E-mail: janas@uakron.edu

The fiber-based high efficiency particulate air (HEPA) filters can effectively remove 99.95 % of particles that are larger than 0.3 μm. The ultra-low penetration absolute (ULPA) filters, patented by George et al. (1996) can capture 99.99999 % of particles 0.1 μm or larger. Both HEPA and ULPA filters are used in industrial settings. However, particles smaller than 0.1 μm still present a challenge for filtration. In personal facemask style respirators, the commonly used P100 respirator is effective to block only 99.9 % of particles 0.3 μm or larger in size. This presents much room for further study and improvement. In this context, the present study ventured into combining woven fabric media with no inherent filtration capability with high filtration efficiency aerogel coatings on the fabric. Such a composite media may offer the flexibility in handling due to the fabric and excellent filtration performance due to the coated aerogel layers. These types of composite filter media were produced in this work by dip-coating the fabric in an appropriate sol before the corresponding sol-gel transition took place. This allowed formation of a layer of porous gel network on the fabric.

The dip-coating process is well-developed for solid, nonporous substrates (Schwartz and White, 1994). The complexity of the problem intensifies when considering dip coating on fibrous or other porous substrates. Dip coating onto fibrous substrates is routinely used in textile industry to improve the properties of the textiles such as weathering and self-cleaning attributes. Sol-gel dip coating onto fibrous substrates is feasible, though complex, with much attention paid to evaporation-induced concentration gradients. The direct mechanisms responsible for final coating thickness are convoluted by many factors in comparison to dip coating on solid substrates (Tang and Yan, 2016). Additional challenges are met when considering dip-coating of porous substates with a sol that subsequently undergoes time-sensitive sol-gel transition process. Specifically, control of solvent evaporation becomes an important factor in the film production from the sol-gel dip coating process. To the best of our knowledge not much is known on dip-coating work for fabrication of aerogel materials. The dip-coating of silica aerogels onto glass slides was studied though the issues of solvent evaporation were still present (Hrubesh and Poco, 1995; Kim and Hyun, 2003).

Several critical questions remained unexplored in prior work. First, can one pick arbitrarily a fabric and a sol-gel system to obtain mechanically robust aerogel-coated filter materials? Second, does solvent evaporation deter porous network formation in the aerogel coating layers? Third, does the composite system offer enough compliance to mechanical deformation? The above questions were investigated in this work by considering a commercially available polyester fabric in conjunction with sol-gel systems originating from thermo-reversible gelation in sPS and three-dimensional polymer chain network formation and chemical imidization in polyimide (PI). The interesting morphology and attractive filtration data of aerogel coated woven fabric developed in this work may facilitate usage of such materials in the design of personal protective equipment, including facemasks.

2 Experimental

2.1 Materials

Syndiotactic polystyrene (sPS) with 98 % syndiotacticity, molecular weight of 300,000 g/mol, density of 1.05 g/cm^3, was purchased in the form of pellets from Scientific Polymer Products Inc. (Ontario, NY, USA). A differential scanning calorimetry study on this grade of sPS yielded a glass transition temperature of 98 °C and peak melting temperature of 273 °C at a scan rate of 20 °C/min (Wang, 2013). Tetrahydrofuran (THF) and toluene (certified ACS) were purchased from Fisher Chemical (Fairlawn, NJ, USA). Benzene (> 99.0 % purity) and chloroform (> 99.8 % purity) were purchased from Sigma-Aldrich (Milwaukee, WI, USA) and 200 proof ethanol was purchased from Decon Laboratories, Inc. (King of Prussia, PA, USA). Consumer grade polyester woven fabric was purchased from Jo-Ann Fabrics (Akron, OH, USA). 2,2'-dimethylbenzidine (DMBZ) was purchased from Shanghai Worldyang Chemical Co. Ltd. (Shanghai, PRC), pyromellitic dianhydride (97 %) (PMDA) was purchased from Alfa-Aesar (Haverhill, MA), and 1,3,5-tris(4-aminophenoxy)-benzene (96 %) (TAB) cross-linker was purchased from Sigma-Aldrich (Milwaukee, WI, USA). Pyridine (certified ACS), acetic anhydride (certified ACS) and acetone (certified ACS) were purchased from Fisher Chemical (Ontario, NY, USA). N,N-dimethylformamide (DMF) was purchased from VWR International (Radnor, PA, USA).

2.2 Preparation of Sol

sPS pellets were added to THF in a hermetically sealed vial to obtain a polymer concentration of 0.05 g/ml. The vial was heated at 170 °C in an oil bath and the content stirred using magnetic stir bars at 1 200 RPM until the pellets dissolved completely. The solution was poured into a mold sealed with vacuum grease and allowed to gel in approximately 12 h. The polyimide gel was synthesized via two-step chemical reactions. First, polyamic acid was synthesized at room temperature by reacting PMDA and DMBZ solutions in DMF by magnetic stirring at 1 200 min^{-1} for 2 min. Second, the polyamic acid was reacted with TAB solution in DMF with additional stirring for 1 min to obtain crosslinked network followed by chemical imidization using acetic anhydride and pyridine for 2 min. Polyimide sol with 8 wt% polymer was synthesized from 0.212 g DMBZ in 1.5 ml DMF, 0.240 g PMDA in 2.5 ml DMF, 0.006 g TAB in 1 ml DMF, and a mixture of 0.710 g acetic anhydride and 0.692 g pyridine. The solution was then transferred to a mold sealed with vacuum grease and allowed to set for approximately 24 h.

2.3 Preparation of Aerogel-Coated Fabric

The fabric substrate was dip-coated in sPS sol by immersing it in the sol at the 4-minute mark after sPS solution was removed from the heat source. The fabric was kept immersed for 1 minute, removed from the solution at retraction rate of 1, 5, and 10 mm/s, and allowed to cool in air for 1 to 5 min to obtain gel-coated fabrics. Finally, the gel-coated fabrics were transferred to ethanol to begin solvent exchange. In the case of dip-coating with PI, the fabric was placed in the solution immediately after acetone and pyridine were added to the polyamic acid solution. The fabric was removed from the sol after 1 minute in an effort to allow the sol to thicken to provide a solid coating and then transferred to a container filled with acetone. Note that 100 % acetone was used in this step; a solution of acetone and DMF was not used as it dissolved the coating.

The sPS coated fabric specimens were placed in 100 % ethanol, followed by exchange with fresh ethanol three times daily, at least two hours apart, for three days. The PI-coated substrates were placed in 100 % acetone for solvent exchange. The fabric specimens coated with sPS gel were annealed in THF vapor to counter the closure of surface pores during handling. For this purpose, the coated fabric specimens were exposed to THF vapor obtained by boiling liquid THF at 60 °C in a closed vial. The vial and fabric cooled naturally at room temperature and annealed fabric specimens were taken out after different elapsed times. The sPS gel-coated fabric was transferred to ethanol for solvent exchange as presented earlier.

2.4 Supercritical Drying

All specimens were supercritically dried in CO_2. For this purpose, specimens were placed inside a pressure chamber and the chamber was filled with liquid CO_2. The specimens were cleansed with liquid CO_2 four times at intervals of 1 hour, 1.5 hour, then twice for 2 h to fully replace the solvent within the gel network. Finally, the temperature was raised to 50 °C and a pressure of 12.5 MPa to obtain supercritical condition of CO_2 and the gas was vented after 1 hour to obtain aerogel specimens.

2.5 Characterization

The morphology of aerogel-coated fabric was examined using a scanning electron microscope (SEM, model JSM-7401F, Jeol, Peabody, MA, USA) at an operating vol 2 kV and 5 kV respectively for specimens of sPS and PI. Bulk density (r_b) was calculated from Eq. 1 from mass (m) and volume data.

$$\rho_b = m/(w \times h \times t). \tag{1}$$

In Eq. 1, w, h, and t represent the width, height, and thickness of the materials. Skeletal density (r_s) was obtained via Accupyc 1340 Helium Pycnometer (Micrometrics Instrument Corp., Norcross, GA, USA). Porosity (Π) was calculated from the values of bulk and skeletal density as in Eq. 2.

$$\Pi = \left(1 - \frac{\rho_b}{\rho_s}\right) \times 100\%. \tag{2}$$

The thermal stability of the aerogel-coated fabric specimens was examined using TA Hi-Res 2950 (TA Instruments, New Castle, DE, USA) thermogravimetric analyzer (TGA) at a scan rate of 10 °C/min under nitrogen. Micromeritics Tristar II 3020 Analyzer (TA Instruments) was used to obtain specific surface area and pore size distribution in fabric specimens. Adsorption-desorption isotherms of nitrogen at 77 K and CO_2 at 273 K were obtained. Surface area was calculated using the Brunauer-Emmett-Teller (BET) method and pore size distribution was calculated using the nonlocal density functional theory model. The volume of mesopores (V_{Me}) and micropore (V_{Mi}) data were obtained from BET analysis of nitrogen and carbon dioxide adsorption data. Macropore volume (V_{Ma}) was obtained from total pore volume (Vp, Eq. 3), V_{Me}, V_{Mi} as in Eq. 4.

$$V_P = \frac{1}{\rho_b} - \frac{1}{\rho_s}. \tag{3}$$

$$V_{Ma} = V_p - V_{Me} - V_{Mi}, \tag{4}$$

The fractions of micropore (Φ_{Mi}), mesopore (Φ_{Me}), and macropore (Φ_{Ma}) are obtained using Eqs. 5 to 7.

$$\Phi_{Mi} = \frac{V_{Mi}}{V_P}, \tag{5}$$

$$\Phi_{Me} = \frac{V_{Me}}{V_P}, \tag{6}$$

$$\Phi_{Ma} = \frac{V_{Ma}}{V_P}. \tag{7}$$

2.6 Air Permeability and Filtration Efficiency

An air permeability tester (Frazier Precision Instrument, Hagerstown, MD, USA) was used. The relationship between volumetric flowrate (Q) and pressure drop (ΔP) was recorded and Darcy's law (Eq. 8) was used to obtain a value of air permeability (k) from the flow area (A) and thickness (L) of the specimen and air viscosity (μ).

$$\frac{Q}{A} = \frac{k}{\mu}\frac{\Delta P}{L}. \tag{8}$$

Filtration efficiency (Eq. 9) was determined using a filter tester (model TSI-8130, TSI Inc., Shoreview, MN, USA) with an accuracy of 99.999 % from the data on the fraction of particles captured after a five second pass through the filter medium. Airborne sodium chloride nanoparticles with size 25 to 150 nm and average diameter of 75 nm were generated in the instrument and detected before and after passing through the filter materials with a laser photometer. In Eq. 9, N_i and N_o represent the number of particles before and after passing through the filter respectively.

$$E = \frac{N_i - N_o}{N_i} \times 100\%. \tag{9}$$

3 Results and Discussion

The aerogel-coated fabric substrates were analyzed to determine the following attributes – flexibility and mechanical integrity of the substrates, bulk density, porous nature of the coated layers in relation to parent aerogel monoliths, and air permeability and filtration efficiency of airborne nanoparticles. The results will qualify if such materials can be considered for the design of personal protective gears for protection against airborne living organisms of a few tens of nanometer in size. In this context, air permeability and filtration efficiency are equally important. As will be discussed later, the artifact of dip-coating method interfered with the pore architecture of the aerogel coating layer, which was mitigated in this work by an additional solvent vapor annealing step.

3.1 Quality of Aerogel-Coated Fabric Substrates

A set of representative images of aerogel-coated fabric specimens are presented in Fig. 1. The PI aerogel coating easily frac-

tured upon crimping of the coated fabric (Fig. 1A), while the sPS aerogel coating was more compliant to mechanical deformation with no visible damage in the aerogel layer (Fig. 1B).

The SEM images presented in Fig. 2 indicate the morphology of sPS and PI aerogel-coated fabric specimens. The internal structure of the polyester woven fabric is shown in Fig. 2A. The woven structure of the fabric produced wicking of the polymer solution in the dip coating process. Figure 2B shows an SEM image of a fabric dip-coated in hot sPS solution at 100 °C, held to cool for three minutes, thus allowing sPS solution to cool and turn into gel state. It is evident from Fig. 2B that wicking by sPS solution led to complete coverage of the fabric. The SEM image in Fig. 2C shows a magnified view of the morphology of surface pores in an sPS *aerogel monolith*, formed by allowing the solution to cool and turn into gel within a sealed mold for up to 12 h. This image will serve as a reference for examining the magnified view of surface morphology of sPS aerogel-coated fabric produced via dip-coating method. A comparison of the morphologies of polyimide aerogel monolith (Fig. 2D) and polyimide aerogel coated fabric (Fig. 2E) indicate ample surface pores on PI aerogel-coated fabrics. In view of the visible fracture seen in Fig. 1A, we conclude that the PI aerogel formulation used in this work did not produce mechanically robust aerogel-coated fabric although the pore morphology of PI aero-

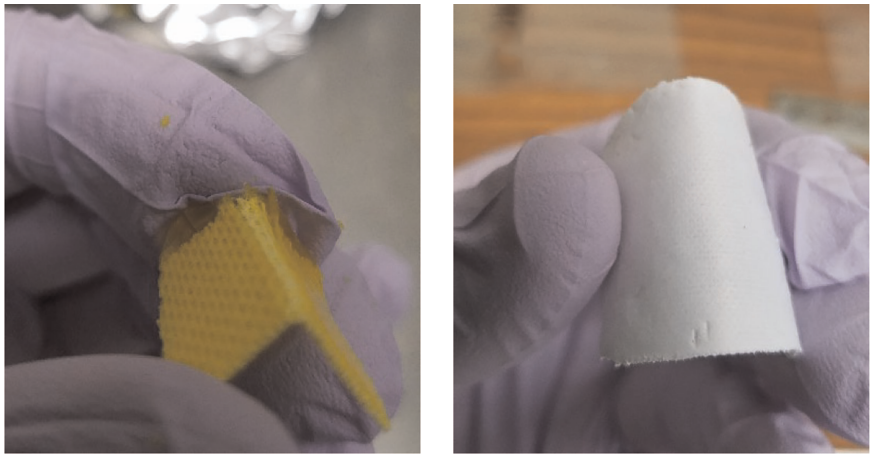

A) B)

Fig. 1. Optical images of aerogel-coated fabric specimens, A) PI-coated, B) sPS-coated

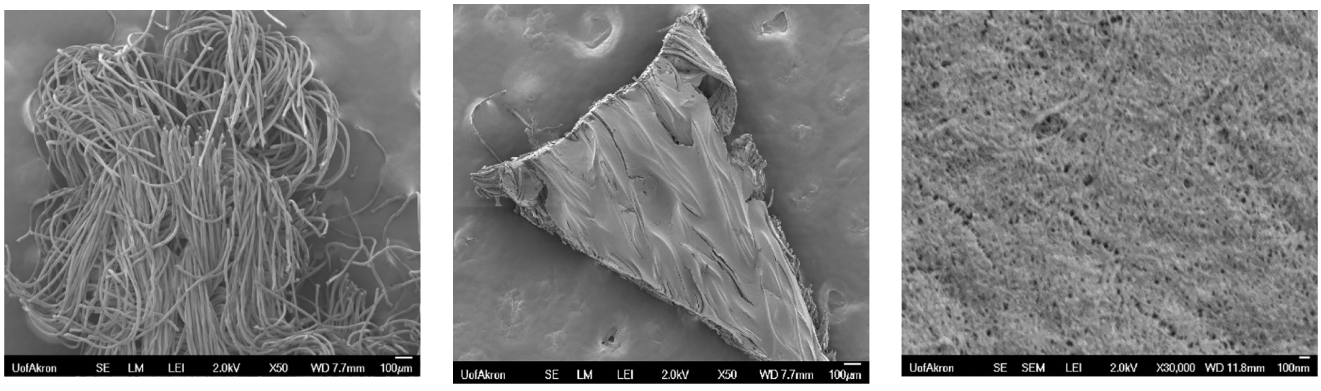

A) B) C)

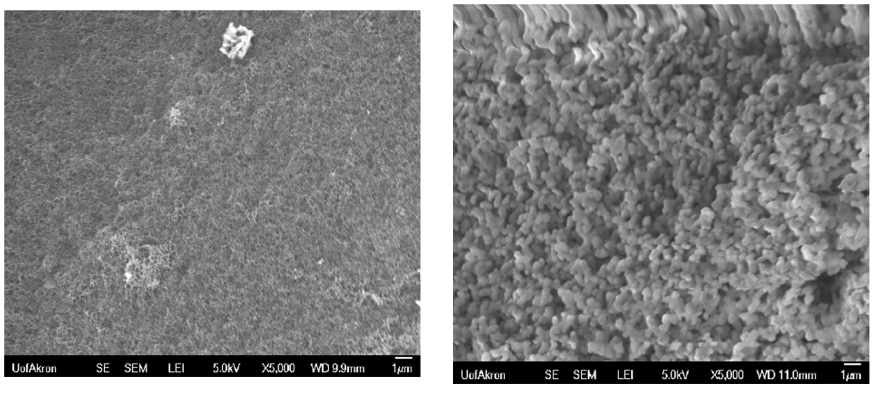

D) E)

Fig. 2. SEM images of (A) polyester fabric, B) sPS aerogel-coated polyester fabric, C) fractured surface layer of sPS aerogel monolith, sPS concentration in (B) and (C) was 0.05 g/ml in THF, D) fractured surface of PI aerogel monolith, and (E) pore structures of PI aerogel-coated fabrics. PI concentration in (D) and (E) was 0.08 g/ml

gel coating layer seen in Fig. 2E indicates acceptable pore morphology. We contend that other PI formulations need to be extensively studied to obtain desired mechanical integrity. In view of this, the rest of the paper discusses only the sPS system.

Figure 3 shows SEM images of the surfaces of sPS aerogel-coated fabrics as function of the time that the coated fabric was exposed to room air for cooling and gelation before subjecting to solvent exchange in ethanol. We note that the liquid layer that coated onto the fabric substrate maintained low viscosity until its temperature reduced to trigger sol-gel transition at approximately 60 °C. If the fabric is dipped into ethanol prematurely, the sPS chains precipate without forming a layer of gel coating on the fabric. A visual examination of the coating layer thickness in Fig. 3 indicates that sPS sol needed a critical elapsed time to turn into a gel before the gel-coated fabric could be solvent exchanged in ethanol. For example, polyester fabric ends are clearly visible in Fig. 3A for specimens that were kept in room air for only 1 minute. The coverage by sPS gel increased due to higher degree of gelation for a cooling time of seven minutes. The images in Fig. 3B to D show that the cooling times of 3 to 7 min were sufficient for solutions to cool down to sol-gel transition temperature. However, exposure of hot solutions of sPS already coated on the fabric to air during cooling period also allowed significant solvent evaporation which in turn altered the surface pore morphology. The surface pore structures are not clearly visible in Fig. 3B to D even at a magnification of 15,000. As will be discussed later, the surface pores could be maintained by exposing sPS solution-coated fabric specimens to THF vapor during the cooling period.

3.2 Aerogel Coating Thickness

Table 1 lists thickness of sPS aerogel coating layers on fabrics. Three sets of specimens were produced by dipping three fabric specimens of known thickness in sPS solution of the same polymer concentration of 0.05 g/ml and retracted at a known speed, e. g., 1 mm/s, 5 mm/s, and 10 mm/s. For each specimen thus produced, the thickness was measured at five arbitrary locations to obtain an average value. In traditional dip-coating

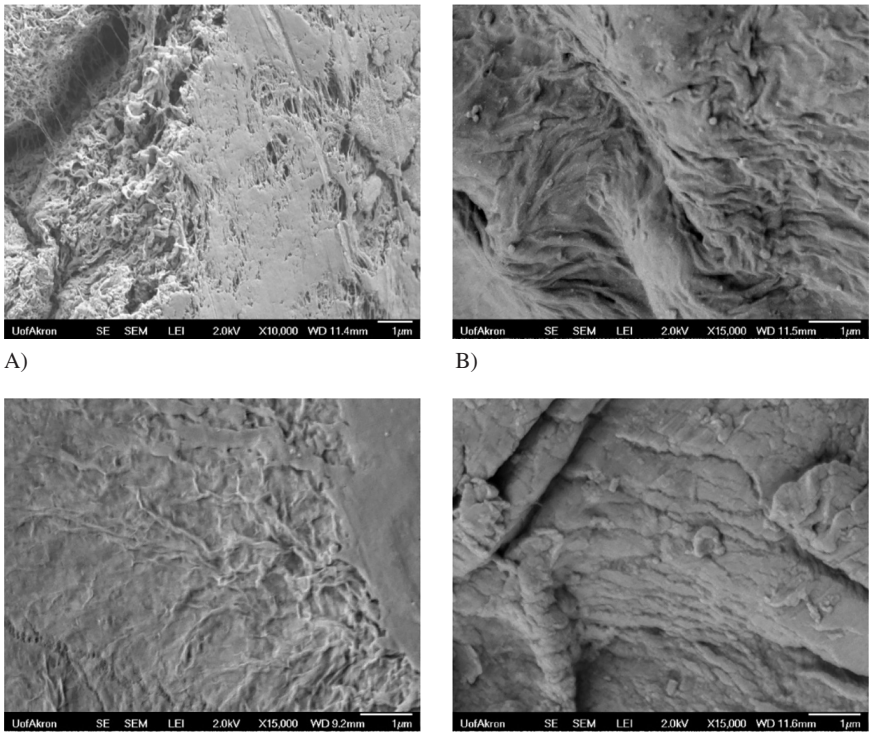

Fig. 3. SEM image of surface of polyester fabric coated with aerogel synthesized as 0.05 g/ml sPS in THF and then air dried for A) 1, B) 3, C) 5, D) 7 min respectively

	Uncoated fabric	Retraction speed		
		1 mm/s	5 mm/s	10 mm/s
Average thickness series 1 (mm)	0.34 ± 0.031	0.42 ± 0.024	0.43 ± 0.011	0.42 ± 0.040
Average thickness series 2 (mm)	0.35 ± 0.029	0.45 ± 0.029	0.47 ± 0.021	0.43 ± 0.013
Average thickness series 3 (mm)	0.34 ± 0.036	0.44 ± 0.036	0.42 ± 0.020	0.42 ± 0.029

Table 1. Thickness of sPS aerogel coating as function of retraction rate from solution followed by drying for 3 min

process involving nonporous substrates, the retraction rate was found to be one of the most influential parameters in controlling the thickness of the gel (Schwartz and White, 1994). The data in Table 1 show that the retraction rate had no apparent influence on coating thickness. This is likely due to rapid wicking of the fabric by the low viscosity sPS solution. The porous nature of the substrate promoted ingress of sPS solution assisted by high capillary pressure over a timescale much shorter than the time of dipping (1 minute). The data in Table 1 establish that retraction rate was not an important factor in deciding the thickness of the coating. It is inferred that the aerogel coating thickness varied in the range of 0.07 to 0.11 mm.

The TGA data (not included) conducted under nitrogen showed that sPS lost most of its weight at ~325 °C, while the fabric showed significant weight loss at ~360 °C. At 290 °C, the sPS lost 2 % of its initial weight, while the fabric did not lose any weight at this temperature. The sPS aerogel-coated specimen weight loss occurred in two steps, first at 325 °C due to loss of sPS and then in the range of 355-365 °C, due to loss of fabric material. In view of the above data, the aerogel coated fabric can be used without any weight loss at 290 °C, although crystalline sPS undergoes melting at around 270 °C.

3.3 Density and Porosity

The skeletal density of the polyester fabric and sPS were determined by helium pycnometry to be respectively 1.48 g/cm^3 and 1.05 g/cm^3. The skeletal density of sPS aerogel-coated fabric varied in the range of 1.21 to 1.30 g/cm^3. One can conduct mass balance to determine sPS content in the resultant fabric, which varied in the range of 33 to 53 wt%. The bulk density of sPS aerogel and polyester fabric were measured to be respectively 0.06 g/cm^3 and 0.2880 g/cm^3, while the bulk density of sPS aerogel-coated fabric was in the range of 0.34 to 0.36 g/cm^3. Accordingly, the aerogel-coated fabrics had porosity of 71 to 73 % compared to a porosity of ~80 % of the fabric, calculated using Eq. 2. The small reduction of porosity in aerogel-coated fabric was due to filling of some of the pores of the fabric by sPS chains. An additional reduction originated from the reduction of mesopore fraction as discussed below.

3.4 Specific Surface Area and Porosity

The BET data presented in Fig. 4 show hysteresis loops indicating the presence of significant mesopores. It is noted that the area under the hysteresis loop and the quantity of gas absorbed reduced in the case of materials cooled over a longer time (3 and 5 min), indicating loss of mesopore fraction due to pore collapse. The data on specific surface area, pore volume, and the composition of different pores are listed in Table 2. The specific surface area and pore volume reduced considerably in sPS-aerogel coated fabrics compared to sPS aerogel monolith although, as seen above, sPS constituted 33 to 53 wt% of the aerogel-coated fabric. The specific surface area and pore volume of sPS aerogel monolith were respectively 306 m^2/g and 15.7 cm^3/g. These values for aerogel-coated fabric reduced with an increase of cooling time, e. g., 82 m^2/g specific surface area, 2.0 cm^3/g pore volume at 1 minute of cooling to specific surface area of 42 m^2/g and pore volume of 2.0 cm^3/g at 3 min of cooling time.

It is known from prior work (Daniel et al., 2005) that the small micropore fractions in sPS aerogels, as determined from CO_2 adsorption-desorption isotherms, originate from the cavities in helicoidal polymer strands. In this work, the micropore fraction reduced from 0.3 vol% in sPS aerogel to 0.1 to 0.2 vol% in sPS-coated fabric. It is noted that the micropores do not make any impact on airborne nanoparticle filtration and that mesopore and macropore fractions are significantly more important in determining filtration efficiency and air permeability respectively (Kim et al., 2016; Zhai and Jana, 2017). The data in Table 2 show that mesopore fractions (2.2 to 2.4 vol%) in sPS aerogel-coated fabrics cooled in air for 3 and 5 min are comparable to mesopore fraction (2.8 vol%) of sPS aerogel monolith. These materials also show macropore volume content of ~97 %. The fabric cooled in air for 1 min

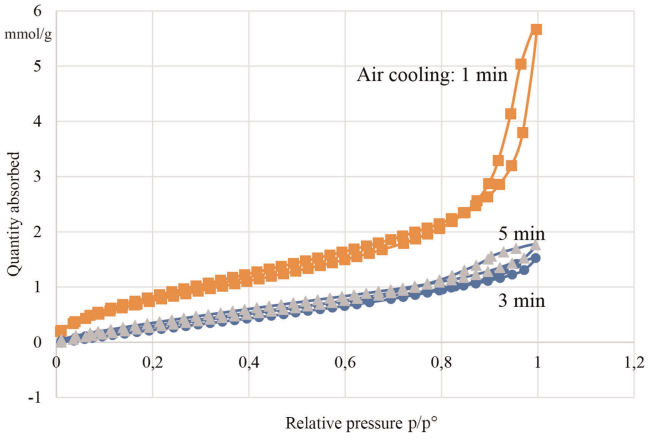

Fig. 4. Nitrogen sorption isotherms of the air cooled, sPS aerogel-coated fabrics

	sPS aerogel monolith	Coated fabric after 1 min air cooling	Coated fabric after 3 min air cooling	Coated fabric after 5 min air cooling
Surface area (m^2/g)	306	82	42	44
Pore volume (cm^3/g)	15.7	2.0	2.0	2.2
Micropore (vol%)	0.3	0.20	0.1	0.1
Mesopore (vol%)	2.8	7.5	2.2	2.4
Macropore (vol%)	96.9	92.3	97.7	97.5

Table 2. BET surface area and pore fractions

shows much higher mesopore fraction (7.5 vol%) and macropore fraction of 92 vol%. These data will be revisited while discussing airborne nanoparticle filtration data.

3.5 Permeability

Table 3 lists data on air permeability and efficiency of airborne nanoparticle filtration. These data reveal several trends. First, the aerogel-coated fabric prepared by cooling in air for 1 minute shows air permeability ($\sim 10^{-8}$ m^2) about two orders of magnitude higher than sPS monolith (10^{-10} m^2) and four orders of magnitude higher (10^{-12} m^2) than aerogel-coated fabric prepared by cooling in air for 3 and 5 min. It was inferred earlier from the SEM image presented in Fig. 3A that aerogel coating on polyester fabric was not complete by 1 minute of air cooling, thus leaving large gaps in the coating, which led to very high permeability. In the case of air cooled samples for 3 and 5 min, the permeability values were two orders of magnitude lower than that the of aerogel monolith due to the large amount of pore collapse that occurred as a result of solvent evaporation, particularly at the top and bottom surfaces. Second, 1-minute air cooled sample offered low particle filtration efficiency of 24 % compared to 99.999 % for sPS aerogel monolith. The fabric specimens obtained by cooling for 3 and 5 in air show higher filtration efficiency of respectively 85 % and 79 %.

3.6 Effects of Solvent Annealing

The SEM images included in Fig. 5 show the morphology of the surfaces of sPS aerogel-coated fabrics after supercritical drying. Recall that the corresponding gel-coated fabric specimens were exposed to THF vapor and allowed to cool naturally for variable amounts of time. The image in Fig. 5A shows that allowing the material to remain for 1 minute in contact with THF vapor resulted in a more porous surface of the membrane compared to the aerogel-coated membrane without solvent annealing, seen in image in Fig. 3A. Note that withdrawal of the specimen from the annealing chamber in just 1 minute did not allow the sPS solution to cool enough to gel completely. Thus, upon transferring to ethanol, a part of sPS chains rapidly precipitated and did not participate in producing proper aerogel coating. Figure 5B corresponds to the coated fabric that was held in THF vapor for 3 min. It is apparent that the surface morphology shows some resemblance with that of the sPS monolith (Fig. 2C). The presence of pores on the surface indicates that exposure to THF vapor prevented excessive solvent

	sPS 5 % aerogel monolith	1 min air cool	3 min air cool	5 min air cool
Permeability (m^2)	6.62×10^{-10}	3.39×10^{-8}	8.21×10^{-12}	5.84×10^{-12}
Filtration efficiency (%)	99.999	24.000	85.000	79.000

Table 3. Air permeability and filtration efficiency

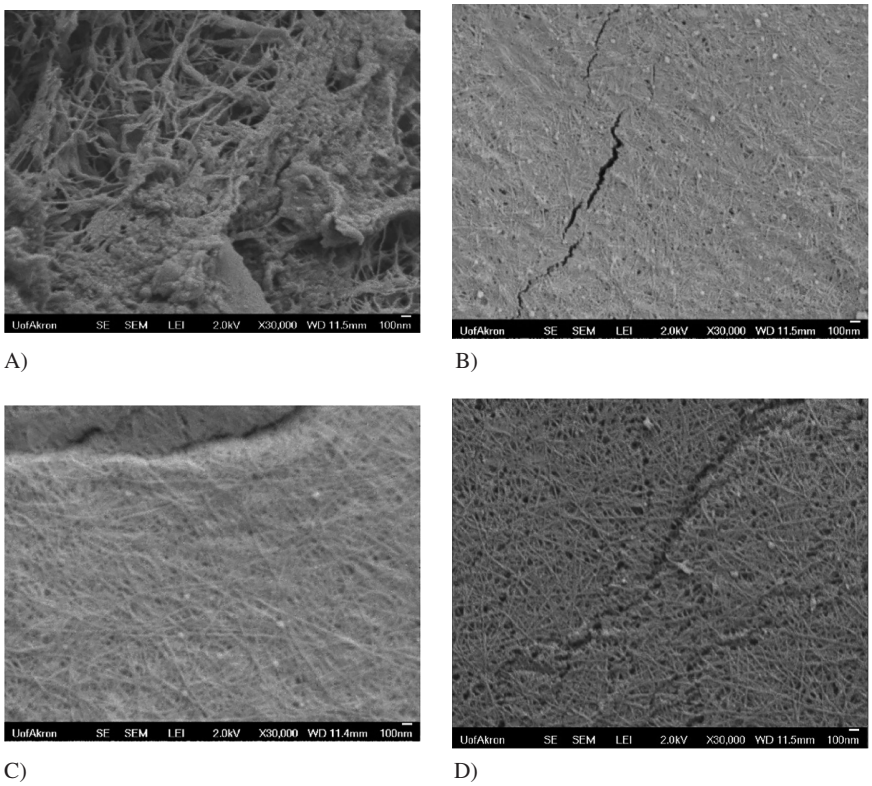

Fig. 5. SEM image of the surface of polyester fabric coated with sPS aerogel from 0.05 g/ml sPS solution in THF and solvent annealed for A) 1, B) 3, C) 5, and D) 7 min

	Uncoated fabric	3 min anneal	5 min anneal	7 min anneal
Average thickness series 1 (mm)	0.35 ± 0.025	0.45 ± 0.032	0.40 ± 0.015	0.47 ± 0.0416
Average thickness series 2 (mm)	0.34 ± 0.031	0.43 ± 0.025	0.42 ± 0.010	0.43 ± 0.050
Average thickness series 3 (mm)	0.34 ± 0.033	0.46 ± 0.029	0.44 ± 0.020	0.44 ± 0.031

Table 4. Effect of annealing in THF vapor on fabric thickness

	sPS monolith	3 min	5 min	7 min	P95	P100
Bulk density (g/cm^3)	0.060	0.316	0.321	0.340	0.164	0.142
Skeletal density (g/cm^3)	1.0611 ± 0.0100	1.3215 ± 0.0219	1.3131 ± 0.0209	1.3510 ± 0.0336	1.2948 ± 0.0063	1.0893 ± 0.0040
Porosity (%)	94	76	76	75	87	87

Table 5. Density and porosity data of solvent annealed specimens

evaporation from the specimen surface and thus prevented pore collapse contrary to what was seen in Fig. 3.

Figures 5C and D show additional pores on the specimen surfaces, even more than what was seen in sPS monolith (Fig. 2C). These images indicate that sPS underwent unhindered gelation at the surfaces. The images in Figs. 5C, D also indicate an unexpected effect of solvent vapor annealing. The surfaces now show population of long fibrillar strands of sPS crystalline domains covering almost the entire surfaces in SEM images. These strands are not present in Fig. 5A or in images of specimens that were not solvent vapor annealed, including the sPS monolith (Fig. 2C). We hypothesize that two different effects occurred due to exposure to THF vapor. First, sPS solution in liquid layer on the fabric cooled and formed a gel without much solvent evaporation in the presence of THF vapor. This also prevented pore collapse due to capillary stress of the evaporating liquid. Second, additional amorphous sPS chains underwent crystallization and formed long fibrils evident in Figs. 5C, D in the presence of hot THF vapor. Specifically, earlier work revealed that the amorphous regions of sPS transition into the all-trans (T4) planar zigzag chain conformation, β- modifications, when exposed to high pressure and heat during supercritical drying step (Sun et al., 1992; Lin and Woo, 2000).

It was seen during experiments that THF vapor condensed on fabric surfaces and dripped off the surfaces of the samples inside the solvent chamber. This raises a question on the effect of duration of solvent annealing time on the thickness of the final composite, especially if condensed liquid THF dissolved the gel from the original coating. However, close values of the specimen thickness data presented in Table 1 without annealing and those in Table 4 with annealing establish that the thickness of the aerogel coating (0.05 to 0.12 mm) did not depend on the annealing time. This is expected as the amount of liquid clinging to the polyester fabric was determined by the dip-coating process.

The values of density and porosity are listed in Table 5 along with two commercially available personal filtration media, recovered from P95 and P100 respirators, as references. It is apparent that bulk and skeletal density and porosity of solvent annealed specimens do not show a clear dependence on annealing times. The skeletal density was determined by the amount of sPS in the coated fabric, which varied from 24 wt% for 7-minute annealed fabric to 29 wt% for 3-minute and 32 wt% for 5-minute annealed specimens. Recall that sPS-coated fabric specimens produced without solvent annealing had 33 to 53 wt% sPS. In view of this, the specimens obtained by vapor annealing had more consistent sPS content.

	3 min anneal	5 min anneal	7 min anneal
Surface area (m^2/g)	25	52	51
Pore volume (cm^3/g)	2.27	2.33	2.20
Micropore (%)	0.36	0.37	0.39
Mesopore (%)	2.20	7.29	7.34
Macropore (%)	97.44	92.35	92.27

Table 6. Surface area and pore volume fraction of annealed aerogel-coated fabric

It is noted from the data in Table 5 that the skeletal density of P95 material is very close to those of solvent vapor annealed aerogel-coated fabric. The porosity was the highest for sPS monolith (94 %) and the lowest (74 to 76 %) for solvent vapor annealed aerogel-coated fabric. The reference materials P95 and P100 offered about 10 % higher porosity than the aerogel-coated fabric.

The values of surface area and pore volume are listed below in Table 6. It is evident from the data presented in Table 6 that specific surface area of solvent vapor annealed, aerogel-coated specimens were substantially lower (25 to 52 m^2/g) compared to $\sim$ 300 m^2/g for the sPS monolith. Note that the macroporous fabric had negligible specific surface area. It is also evident that the macropore fraction (92 to 97 %) did not change much with solvent vapor annealing time and is close to that of sPS monolith (97 %). The mesopore fraction, however, increased substantially

due to solvent vapor annealing. For example, the mesopore fraction increased from 2.2 % with 3 min annealing to 7.3 % for 5 min or longer annealing times. This is also evident in the hysteresis loops seen present in the nitrogen adsorption isotherms in Fig. 6. The sPS aerogel monolith had about 2.8 % of its pore volume in mesopore range. The micropore volume fraction did not change with annealing time as expected.

Air permeability values presented in Table 7 show an increasing trend with annealing time – e. g., 2.36×10^{-11} m^2, 9.76×10^{-11} m^2, and 3.35×10^{-10} m^2 for annealing time of 3, 5, and 7 min, in the same neighborhood of sPS aerogel monoliths (10^{-10} m^2). This can be attributed to the absence of pore closure in the surface layer. Additional surface pores were formed in the presence of solvent vapor due to crystallization of amorphous sPS chains during annealing. One would expect that the presence of more open pores in annealed specimens would also influence filtration efficiency. It is also worth noting that while the intrinsic permeability values of the commercially available filters (P95 and P100) were an order of magnitude or more higher than those of the prepared samples, the commercial filters were also an order of magnitude or more thicker. Thus, in terms of flow rate to pressure drop ratios, the solvent vapor annealed materials performed reasonably well.

For reference, the filtration efficiency of the uncoated fabric was functionally zero, while its permeability value was too high to be recorded via the instruments available. The increase in filtration efficiency with an increase of annealing time from 3 min to 5 min can be attributed to a large increase in mesopore fraction (Table 6) as reported by Kim et al. (2016). A slight increase in mesopore fraction from samples annealed for 5 min to 7 min produced an increase of filtration efficiency from 99.811 % to 99.993 %. The higher permeability of the annealed sample for 7 min should result in a lower pressure drop, thus allowing a better interception of incident particles during air flow (Liu and Wang, 2007). In comparison, the commercial filtration materials P95 and P100 showed slightly lower efficiency than the aerogel-coated fabric.

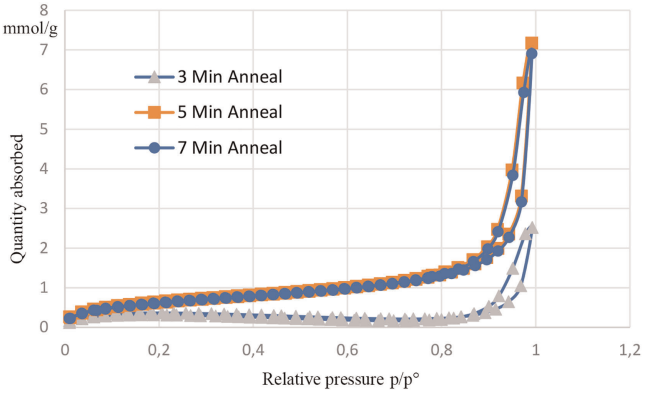

Fig. 6. Nitrogen sorption isotherms of the solvent annealed, aerogel-coated fabrics

	3 min anneal	5 min anneal	7 min anneal	P95	P100
Permeability (m^2)	2.36×10^{-11}	9.76×10^{-11}	3.25×10^{-10}	1.23×10^{-9}	1.41×10^{-9}

Table 7. Permeability values of annealed aerogel coated fabric and commercially available personal filtration devices

4 Conclusions

The study established that polyester fabrics can be easily dip-coated with syndiotactic polystyrene solution to obtain flexible and mechanically compliant composite filtration media with sPS aerogel surface layers that offer meso- and macropores for airborne nanoparticle filtration and air permeability. However, the data presented in this paper indicate that care must be exercised to guard against surface pore closures due to solvent evaporation during the mandatory air-cooling step needed for thermo-reversible gelation of sPS chains. The study also established that such pore closures can be avoided by implementing a cooling process in the presence of solvent vapors. Such vapor annealing also helps create additional pores on aerogel layers via crystallization of amorphous sPS chains. The values of air permeability and filtration efficiency achieved with these materials are in acceptable range in reference to the data obtained simultaneously on two commercial filter materials.

References

Alexander, D. D., EP 0507217 (A1) (1992)

Daniel, C., Alfano, D., Venditto, V., Cardea, S., Reverchon, E., Larobina, D., Mensitieri, G. and Guerra, G., "Aerogels with a Microporous Crystalline Host Phase", Adv. Mater., **17**, 1515–1518 (2005), DOI:10.1002/adma.200401762

George, N. A., Sutsko, M. G. and McKenna, D. B., U. S. Patent 5507847 (1996)

Guise, M. T., Hosticka, B., Earp, B. C. and Norris, P. M., "An Experimental Investigation of Aerosol Collection Utilizing Packed Beds of Silica Aerogel Microspheres", J. Non-Cryst. Solids, **285**, 317–322 (2001), DOI:10.1016/S0022-3093(01)00473-2

Hrubesh, L. W., Poco, J. F., "Thin Aerogel Films for Optical, Thermal, Acoustic and Electronic Applications", J. Non-Cryst. Solids, **188**, 46–53 (1995), DOI:10.1016/0022-3093(95)00028-3

Kim, G. S., Hyun, S. H., "Synthesis of Window Glazing Coated with Silica Aerogel Films via Ambient Drying", J. Non-Cryst. Solids, **320**, 125–132 (2003), DOI:10.1016/S0022-3093(03)00027-9

Kim, S. J., Chase, G. and Jana, S. C., "Polymer Aerogels for Efficient Removal of Airborne Nanoparticles", Sep. Purif. Technol., **156**, 803–808 (2015), DOI:10.1016/j.seppur.2015.11.005

Kim, S. J., Chase, G. and Jana, S. C., "The Role of Mesopores in Achieving High Efficiency Airborne Nanoparticle Filtration Using Aerogel Monoliths", Sep. Purif. Technol., **166**, 48–54 (2016), DOI:10.1016/j.seppur.2016.04.017

Kim, S. J., Jana, S. C., "Effects of Skin Layers on Air Permeability in Macroporous Polymer Aerogels", Polymer, **126**, 432–436 (2017), DOI:10.1016/j.polymer.2017.03.039

Kim, S. J., Raut, P., Jana, S. C. and Chase, G., "Electrostatically Active Polymer Hybrid Aerogels for Airborne Nanoparticle Filtration", ACS Appl. Mater. Interf., **9**, 6401–6410 (2017), DOI:10.1021/acsami.6b14784

Lin, R. H., Woo, E. M., "Melting Behavior and Identification of Polymorphic Crystals in Syndiotactic Polystyrene", Polymer, **41**, 121–131 (2000), DOI:10.1016/S0032-3861(99)00127-5

Liu, Z. G., Wang, P. K., "Pressure Drop and Interception Efficiency of Multifiber Filters", Aerosol Sci. Technol., **26**, 313–325 (2007), DOI:10.1080/02786829708965433

Mosanenzadeh, S. G., Karamikamkar, S., Saadatnia, Z., Park, C. B. and Naguib, H. E., "PPDA-PMDA Polyimide Aerogels with Tailored Nanostructure Assembly for Air Filtering Applications", Sep. Purif. Technol., **250**, 117279 (2020), DOI:10.1016/j.seppur.2020.117279

Pfeffer, R., Quevedo, J., US Patent 8 632 623 B2 (2014)

Quevedo, J., Patel, G., Pfeffer, R. and Dave, R., "Agglomerates and Granules of Nanoparticles as Filter Media for Submicron Particles", Powder Technol., **183**, 480–500 (2008), DOI:10.1016/j.powtec.2008.01.020

Schwartz, L., White, L., "Modelling of the Dip-Coating Process", SOLA Optical, Study Group Report, 109–123 (1994), http://miis.maths.ox.ac.uk/miis/470/1/Modelling-of-the-dip-coating-process.pdf

Sun, Z., Morgan, R. J. and Lewis, D. N., "Crystallization of Syndiotactic Polystyrene under Pressure", Polymer, **33**, 660–661(1992), DOI:10.1016/0032-3861(92)90749-M

Tang, X., Yan, X., "Dip-Coating for Fibrous Materials: Mechanism, Methods and Applications", J. Sol-Gel Sci. Technol., **81**, 378–404 (2017), DOI:10.1007/s10971-016-4197-7

Wang, X., "Tailoring of Pore Structures and Surface Properties of Syndiotactic Polystyrene Aerogels", PhD Dissertation, University of Akron, Akron (2013), DOI:10.1021/la400492m

Zebida, O. A.: Aerogel Filters for Removal of Nanometric Airborne Particles, LAP Lambert Academic Publishing, (2011), ISBN-10 : 9783845441498

Zeng, Z., Ma, X. Y. D., Zhang, Y., Wang, Z., Ng, B. F., Wan, M. P. and Lu, X., "Robust Lignin-Based Aerogel Filters: High-Efficiency Capture of Ultrafine Airborne Particulates and the Mechanism", ACS Sustainable Chem. Eng., **7**, 6959–6968 (2019), DOI:10.1021/acssuschemeng.8b06567

Zhai, C., Jana, S. C., "Tuning Porous Networks in Polyimide Aerogels for Airborne Nanoparticle Filtration", ACS Appl. Mater. Interfaces, **9**, 30074–30082 (2017), DOI:10.1021/acsami.7b09345

Zhang, Y.-G., Zhu, Y.-J., Xiong, Z.-C., Wu, J. and Chen, F., "Bioinspired Ultralight Inorganic Aerogel for Highly Efficient Air Filtration and Oil–Water Separation", ACS Appl. Mater. Interfaces, **10**, 13019–13027 (2018), DOI:10.1021/acsami.8b02081

Date received: February 08, 2021
Date accepted: March 31, 2021

Bibliography
DOI 10.1515/ipp-2020-4095
Intern. Polymer Processing XXXVI (2021) 3; page 322–331

ISSN 0930-777X · 2195-8602